An optimized airfoil geometry for vertical-axis wind turbine applications

Andrés Meana-Fernández*, Lorena Díaz-Artos, Jesús Manuel Fernández Oro

Fluid Mechanics Area, Department of Energy, University of Oviedo
C/Wifredo Ricart s/n Gijón Asturias 33204 Spain

Abstract

In this work, a new airfoil shape optimized for vertical-axis wind turbine applications is proposed. Different airfoil shapes have been analyzed with JavaFoil, a panel method software. Then, the results from the analysis have been used to optimize the performance of the new airfoil shape. Afterwards, Computational Fluid Dynamics (CFD) simulations of the proposed airfoil, UO-17-LDA, are run for different angles of attack to provide insight into the flow field and the mechanisms related to this increase in performance. The UO-17-LDA airfoil presents a high lift-to-drag ratio and a delayed stall angle with respect to the original FX-63-137 airfoil, making it suitable for vertical-axis wind turbine applications. This increase in performance has been verified by comparing two VAWT designs with the original and the proposed airfoil using a double-multiple streamtube model. Finally, the practicality of JavaFoil for the comparison of different airfoil geometries has been verified, as it is capable of obtaining results for a wide number of flow conditions in small computational times and with a user-friendly interface. Nevertheless, the results diverge from the actual solution for high angles of attack (beyond stall). Hence, the time and effort required to perform CFD simulations is justified to gain insight into the actual behavior of a particular airfoil, as well as to obtain a richer analysis of the flow field and the mechanisms related to the airfoil performance.

Keywords: vertical-axis wind turbine; airfoil optimization; panel method, computational fluid dynamics; streamtube model

1. Introduction

In a world in which living without electricity is almost unconceivable, wind energy represents a power source becoming cheaper and more competitive in the course of time. Nowadays, more than 3% of the world energy consumption is supplied by wind energy. This number is expected to rise above 5% in 2020

*Corresponding author: andresmf@uniovi.es

[1]. It is inexhaustible, renewable and non-contaminant. In addition, the use of wind energy helps to reduce the dependence on fossil fuels. For all these reasons, the development of improvements and innovations regarding wind turbines and the aerodynamic airfoils employed to build the blades is a topic of great interest. Wind turbines may be classified with respect to the orientation of the rotor axis in horizontal and vertical axis wind turbines (HAWTs and VAWTs). Although research has been traditionally focused on HAWTs, VAWTs present important advantages, being the main one that they are capable of working independently of the wind direction. In addition, they can produce energy from lower wind speeds, so they can be placed nearer to the ground. This fact makes easier installation and maintenance labors. Besides, the noise level generated by VAWTs is lower. All these advantages make VAWTs especially suitable for their installation in urban areas. On the other hand, VAWTs present some disadvantages that cannot be disregarded, being the main ones the difficulty to self-start and a lower efficiency compared to HAWTs [2]. Due to the continuous changing of the relative position of the blades with respect to the incoming wind, the flow behavior is much more complex than in the case of HAWTs, with the blades working even at stall conditions during part of the rotation cycle. Considering this particular characteristic, the importance of employing an optimized airfoil design for the turbine blades is evident.

Some ideas for the development of better aerodynamic designs may be found in the nature. Biomimicry, the science that studies nature in order to inspire innovative solutions for human problems, is a source of potential ideas to improve existing systems. Examples include the bullet train Shinkansken [3], [4], based on the plunging movement of the kingfisher, or wind turbine airfoils inspired in the flippers of humpback whales [5],[6] or the wings of puffins [7].

In this work, a new airfoil shape optimized for vertical-axis wind turbine applications is proposed. Different airfoil shapes have been analyzed with a panel method, using the results from the analysis in order to optimize the performance of the new airfoil shape. Afterwards, CFD simulations of the proposed airfoil are run for different angles of attack to provide insight into the flow field and the mechanisms related to this increase in performance. This airfoil presents a high lift-to-drag ratio and a delayed stall angle with respect to the previously analyzed airfoil, which makes it suitable for vertical-axis wind turbine applications. Finally, this increase in performance is verified by comparing two different VAWT designs using a double-multiple streamtube model.

2. Airfoil aerodynamics

The characteristics of the aerodynamic airfoil employed to fabricate the blades of a VAWT have a strong influence in the turbine performance. When the incoming wind impinges on an airfoil, it exerts an aerodynamic force. This force may be decomposed in two components: one in the direction of the wind (drag) and other perpendicular to it (lift). The magnitude of these force components depends on its orientation with respect to the incoming wind, as depicted in Figure 1, left.

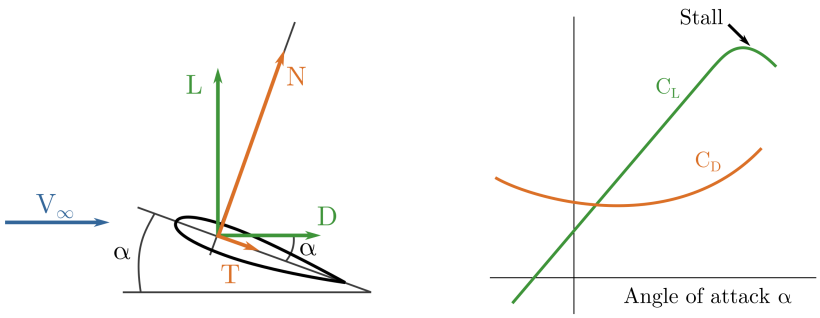

(a) Aerodynamic forces on an airfoil

(b) Lift and drag coefficients as a function of the angle of attack

Figure 1: Basic airfoil aerodynamics

Following this force decomposition, vertical axis wind turbines may be divided in drag-driven and lift-driven wind turbines. Nowadays, lift-driven VAWTs are of much greater interest because the magnitude of lift forces on an airfoil is generally 2 orders of magnitude higher than drag forces. Thus, the main focus of research is the maximization of lift and the reduction of drag in airfoils. These two forces are typically expressed in their dimensionless form:

$$C_L = \frac{L}{\frac{1}{2}\rho S V_\infty^2} \tag{1}$$

$$C_D = \frac{D}{\frac{1}{2}\rho S V_\infty^2} \tag{2}$$

where C_L and C_D are the lift and drag coefficients, L and D are the lift and drag forces, ρ is the air density, S is the cross section of the airfoil and V_∞ is the incoming wind velocity. The main factors affecting the value of these coefficients are the geometry of the airfoil, the angle of attack α between the incoming wind direction and the airfoil chord, and the Reynolds number. Figure 1, right, shows the typical evolution of these coefficients with the angle of attack. Lift generally increases with the angle of attack until reaching the stall angle. At this point, there is a sudden drop in lift with a considerable increase in drag. An airfoil designed for lift-driven turbines should reach high values of lift whilst maintaining low values of drag, and delay stall as long as possible.
The main geometrical characteristics affecting the performance of an airfoil are its maximum thickness, maximum camber and their situation with respect the leading edge of the airfoil. Figure 2 depicts these geometrical features and shows the different parts of a typical airfoil.

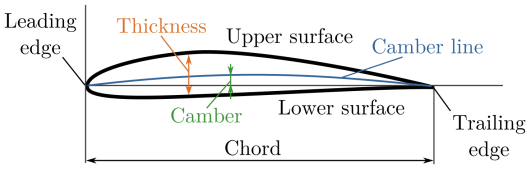

Figure 2: Geometrical features of a typical airfoil

3. Panel methods: JavaFoil

Panel methods are a numerical method for the resolution of potential flow problems. They start from the discretization of the surface of the object under study, introducing an unknown potential term in every surface segment. Then, the influence of the free stream and the relative influences of every potential term are collected in an influence matrix. Finally, solving the equation system formed by this matrix and a vector of geometrical coefficients, the pressure over each segment is obtained and the problem is solved [8].
JavaFoil [9] is a free software that uses a panel method to resolve the velocity and pressure field around aerodynamic airfoils under a flow stream. This software combines the potential flow method with a boundary layer analysis, achieving a good prediction of the aerodynamic behavior of the airfoils at low angles of attack. Due to the simplicity of its interface and its relatively good accuracy with respect to experimental results, it has been chosen for the prediction of the aerodynamic characteristics of airfoils in this study. Nevertheless, after the stall angle, the flow may detach from the airfoil (stall), leading to unreliable results [9]. As the aim of this study is to generate an airfoil geometry that delays stall while maintaining a high value of lift, only the range of angles of attack below the stall angle are to be considered. Thus, JavaFoil is valid for the purpose of this work. The procedure to obtain the airfoil polars is the following: the coordinates of the airfoil are introduced in JavaFoil. Then, the airfoil Reynolds number and the range of angles of attack for the analysis are specified and the calculations are started. With this inputs, the software provides relatively quickly the values of CL and CD for every angle of attack.

3.1. Family of airfoils under study

Table 1 collects the airfoils selected from the bibliography to be analyzed in this study, alongside their particular characteristics. Figure 3 shows the geometry of the airfoils outside the standard NACA family studied in this work.

3.2. Validation of the method

In order to validate the results of the software, two verifications have been performed: firstly, the independence of the discretization of the geometry has been checked using the NACA0012 airfoil at three different Reynolds numbers:

Table 1: Family of airfoils under study

Airfoil	Thickness	Max. thickness position	Camber	Max. camber position
NACA 0012	12%	40%	0%	0%
NACA 0015	15%	40%	0%	0%
NACA 0018	18%	40%	0%	0%
NACA 0021	21%	40%	0%	0%
NACA 2412	12%	40%	2%	40%
NACA 2415	15%	40%	2%	40%
NACA 2418	18%	40%	2%	40%
NACA 2421	21%	40%	2%	40%
DU-06-W-200	19.8%	31.1%	0.5%	84.6%
NACA 23016	16%	30%	1.8%	15%
FX-63-137	13.7%	30.9%	6%	53.3%
NLF(1)-0115	15%	44.1%	1.8%	30%
NLF(1)-1015	15%	39.8%	4.3%	62.8%
S1020	15.1%	33.8%	4.6%	57%
S1012	12%	37.3%	0%	0%
S8037	16%	33.5%	1.9%	40.4%
NACA0012H	12.2%	22.5%	0%	0%

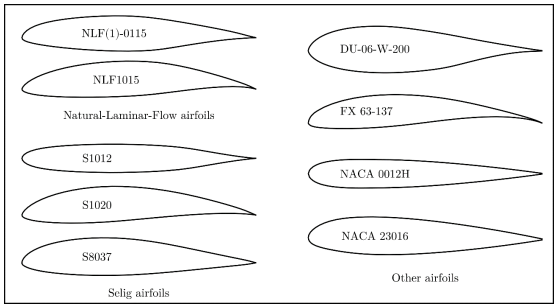

Figure 3: Special airfoils analyzed in this study

20,000, 100,000 and 500,000. It was found that a discretization of 221 points along the surface was adequate enough to ensure the convergence of the results. Secondly, the different 9 transition and 2 stall models (Calcfoil and Eppler) of the software were tested using experimental results of the DU-06-W-200 airfoil to validate the results for the further analyses [10]. The transition model chosen did not seem to affect the results, but the two different stall models did. Figure 4 shows the results of the comparison of the results obtained with the two different stall models at Re=300,000 and 500,000 and the experimental results. It may be appreciated that the results of the software are similar to the experimental ones. The value of the stall angle is captured better by the Calcfoil stall model, but the lift coefficient is more similar to the experimental one with the Eppler model.

For further validation and selection of the stall model, experimental results from a NACA0021 at Re=500,000 have been compared with results from the

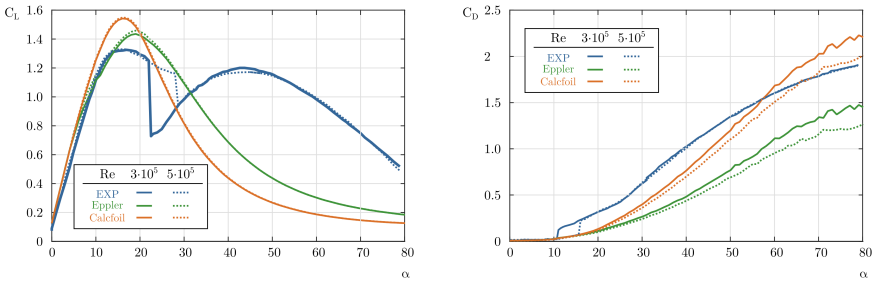

(a) Lift coefficient (b) Drag coefficient

Figure 4: Comparison of experimental and JavaFoil values - DU-06-W-200 airfoil

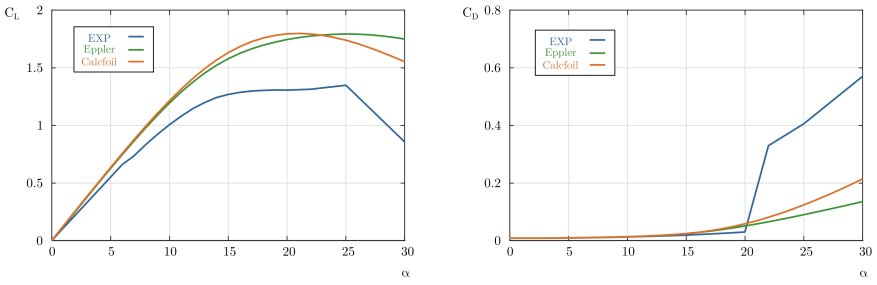

(a) Lift coefficient (b) Drag coefficient

Figure 5: Comparison of experimental and JavaFoil values - NACA 0021 airfoil at Re=500,000

different models. Figure 5 shows this comparison, in which the two models yield values similar to the experimental ones. However, the Calcfoil model seems to follow better the tendency of the experimental results, so this model will be used throughout the rest of the study.
To summarize, JavaFoil yields accurate enough results in the linear part of the lift curve, which start to distance from the experimental results as the airfoil moves toward the stall angle. Nevertheless, the results may be considered as valid for the purpose of preliminary airfoil design and comparison of different airfoil geometries.

3.3. Results

The results from the analysis with JavaFoil of the different airfoils under study are collected in Figures 6, 7, 8 and 9.
For the symmetrical airfoils (Figure 6), it may be observed that the lift coefficient and the stall angle increase with the increase in the airfoil thickness. In addition, when the Reynolds number rises, the lift coefficient increases and the drag coefficient decreases, improving the performance of the airfoil in the linear zone. The stall angle increases as well, widening the useful range of angles of attack of the airfoil.

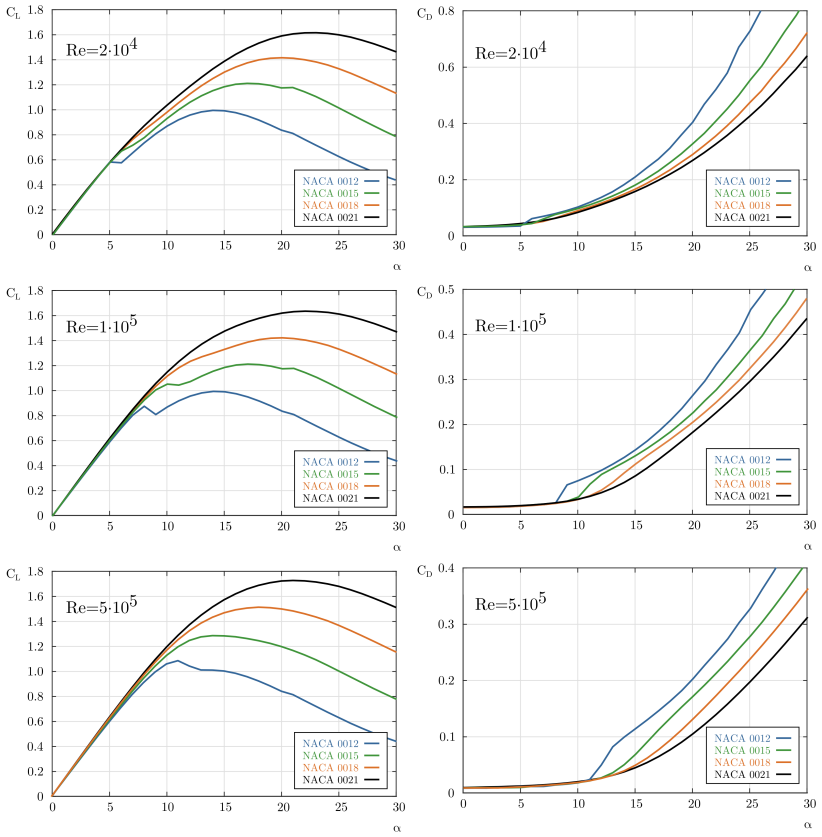

Figure 6: Lift and drag coefficients of the symmetrical NACA airfoils

For the cambered airfoils (Figure 7), the increase of the Reynolds number improves the performance of the airfoil as well. In comparison with the symmetrical airfoils of the same thickness, these cambered airfoils perform better, showing higher values of the lift coefficient with similar values (or just slightly lower) of the stall angle. The global tendency that may be appreciated is the increase of the stall angle and the lift coefficient with the increase in thickness. Adding camber to the airfoils (2%) increases the lift values and decreases the drag ones with respect to the symmetrical airfoil. Although the stall angle decreases slightly in comparison with the symmetric airfoils, the performance of the cambered airfoils is better. Finally, the increase of the Reynolds number causes an increase in C_L and the stall angle and a decrease in C_D.
Following this analysis, the thickness of the airfoil could be increased to delay stall and increase lift, but this would result in an increase of the airfoil weight, increasing its cost as well as the loading in the turbine. Hence, a maximum thickness of 21% has been selected as an optimal value. In Figures 8 and 9, the effect of adding camber may be clearly appreciated. Airfoils with 2% camber

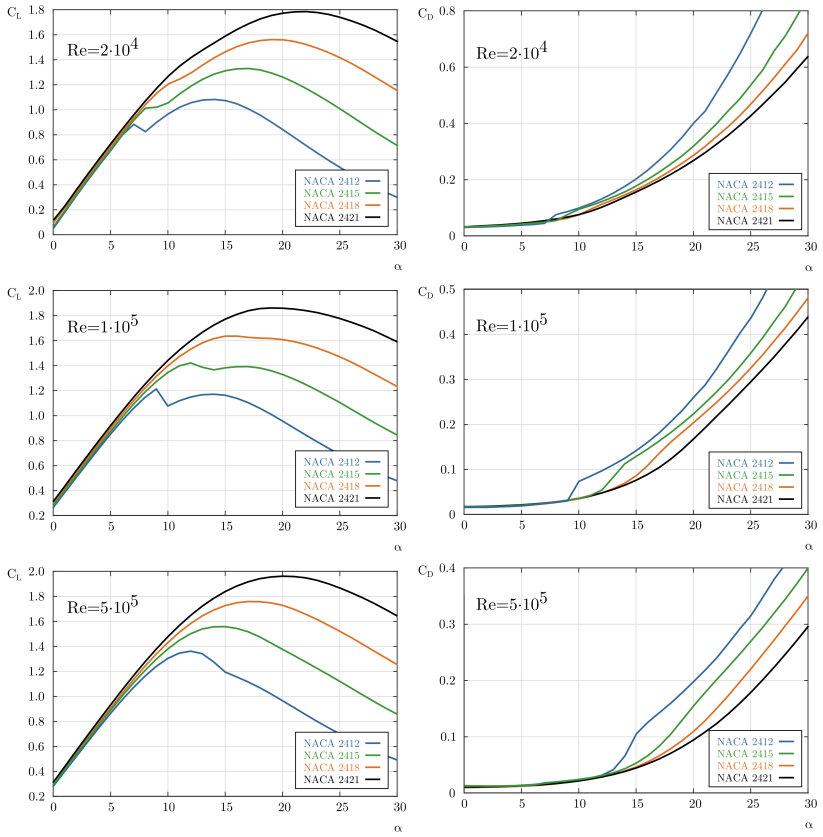

Figure 7: Lift and drag coefficients of the asymmetrical NACA airfoils

show better performance than the symmetrical ones. They present lower values of the stall angle, but they can be considered acceptable. On the contrary, airfoils with 4% or higher camber show very high values of C_L and very low values of C_D, but they present very low values of the stall angle. Thus, for application to vertical-axis wind turbines, it is interesting to use airfoils with a small amount of curvature to ensure both high C_L/C_D ratios and a wider useful range of angles of attack. The airfoils that have shown better aerodynamic performances are the NLF(1)-0115, FX-63-137 and S1012.

3.4. Proposal of an optimized airfoil

Based on the results from the previous section, five different airfoils have been proposed. The thickness and camber of some of the airfoils that presented the best performances were modified. Table 2 shows the geometrical characteristics of the airfoils proposed.

Figure 10 shows the prediction of the performance of the proposed airfoils,

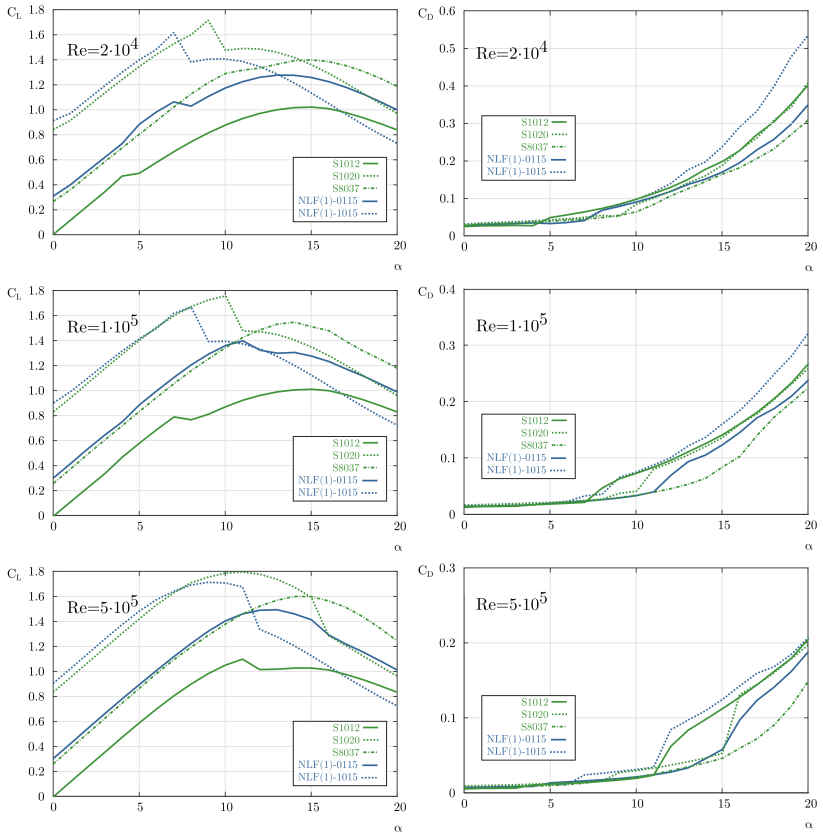

Figure 8: Lift and drag coefficients of the Selig and NLF airfoils

Table 2: Geometrical characteristics of the proposed airfoils

Proposed airfoil	Original airfoil	Thickness	Max. thickness position	Camber	Max. camber position
Airfoil 1	NLF(1)-0115	18%	44.1%	1.8%	30%
Airfoil 2	NLF(1)-0115	21%	44.1%	1.8%	30%
Airfoil 3	FX-63-137	18%	30.9%	2%	53.3%
Airfoil 4	FX-63-137	21%	30.9%	2%	53.3%
Airfoil 5	S1012	18%	37.3%	0%	0%

which present better results than the original ones. Among all the proposed airfoils, Airfoil 4 is the one reaching the highest value of the lift coefficient. This airfoil enters the stall region at $\alpha = 18°$ for $Re = 20,000$ and 16° for the other Reynolds numbers analyzed; hence, it delays well enough stall. In addition, the drag coefficient is not very high at the stall angle; thus, it presents a good C_L/C_D ratio.

Figure 11 compares the performance of the fourth proposed airfoil (hereafter

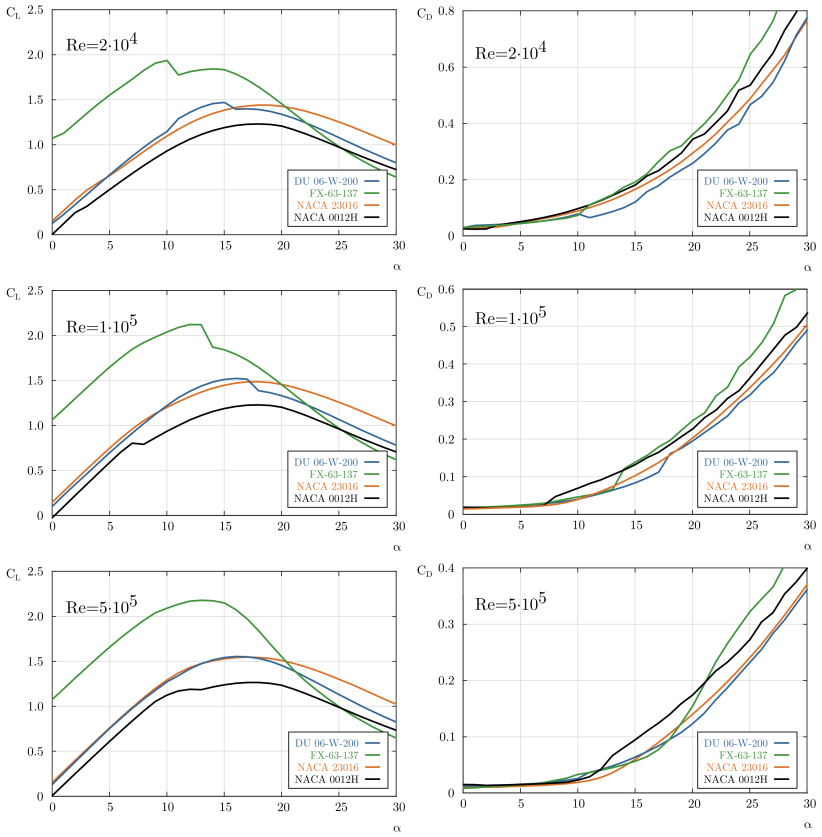

Figure 9: Lift and drag coefficients of other special airfoils

UO-17-LDA) with the original one, FX-63-137. It may be appreciated how the modification performed delays stall. The maximum C_L value of the new airfoil is slightly lower than the value for the original one, but the stall angle has been increased 5°. Regarding the C_D values, although they are very similar until the stall angle for both airfoils, in the proposed airfoil the increase of drag is much less steep. Hence, this proposed airfoil seems more suitable for its use in the wide range of angles of attack that may be found in vertical-axis wind turbines. The geometry of this optimized airfoil is shown in Figure 12.

4. Numerical simulation of the proposed airfoil

In order to gain insight into the flow field and the mechanisms related to the increase in performance of the UO-17-LDA airfoil, CFD simulations of the proposed airfoil have been run for different angles of attack.

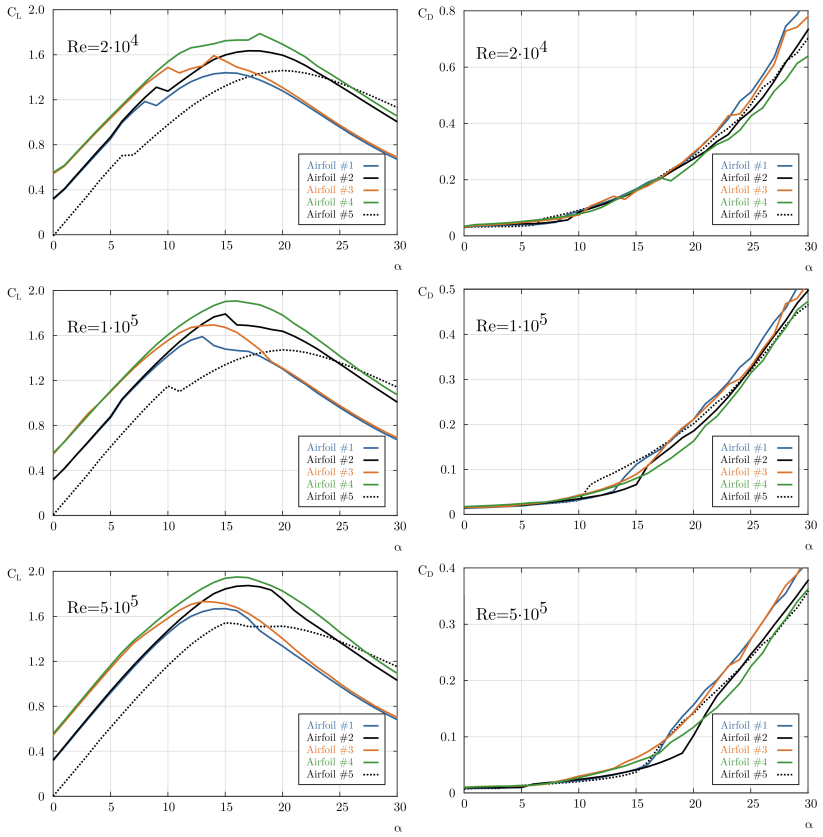

Figure 10: Lift and drag coefficients of the proposed airfoils

4.1. Domain geometry, mesh and boundary conditions

The geometry and mesh have been generated in GAMBIT for a 1 m-chord airfoil, using the same discretization parameters that ensured mesh convergence in the work of [11] . A total number of 116,100 cells have been employed in a 2D model. The boundary layers have been meshed following the guidelines in [12] ensuring a $y^+ < 1$. Figure 13 shows the mesh with a zoom in the airfoil and the leading and trailing edge.

The simulation has been performed at a chord Reynolds number of 500,000. The inlet velocity, corresponding to that Reynolds number, is 7.1 m/s, the pressure outlet is atmospheric pressure and the airfoil is defined as wall. The flow has been simulated at the following angles of attack: -7.5°, -5°, -2.5°, 0°, 2.5°, 5°, 7.5°, 10°, 15° and 20°.

4.2. Numerical solver

The Navier-Stokes equations have been solved in an incompressible fashion using the commercial software ANSYS-FLUENT®. The k-omega SST model

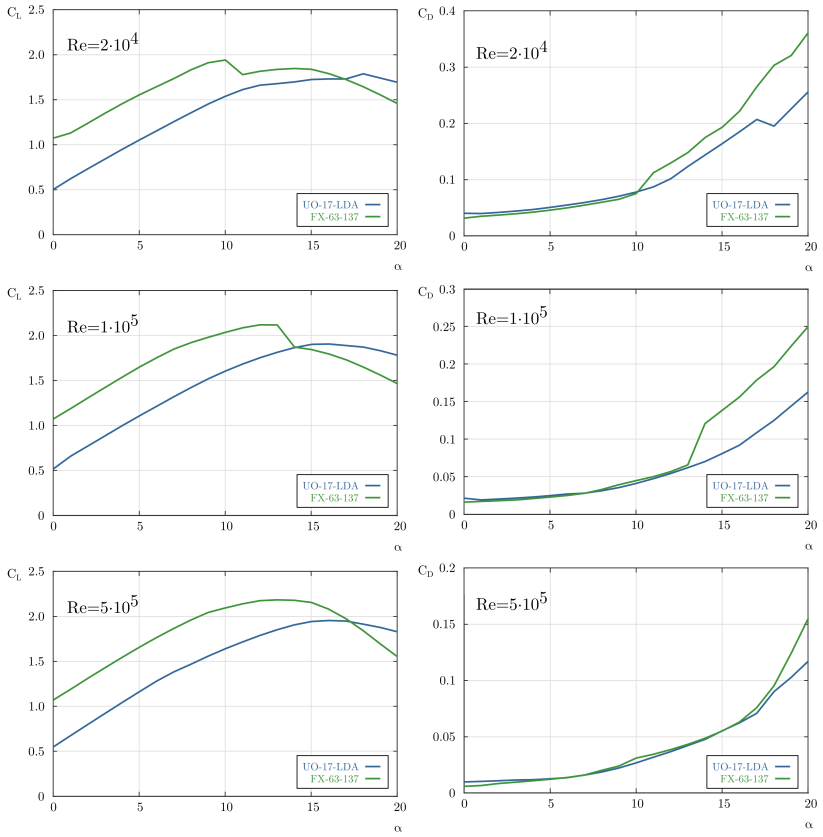

Figure 11: Enhancement of the performance of the new airfoil UO-17-LDA with respect to FX-63-137

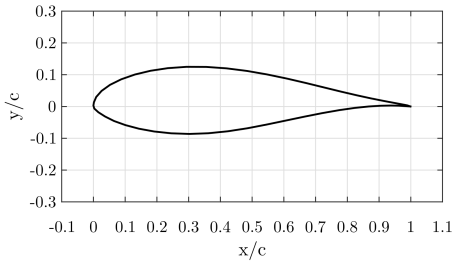

Figure 12: Geometry of the proposed airfoil UO-17-LDA

has been used for the closure of turbulence [13], as it is well adapted to low-Reynolds flows with adverse pressure gradients [14]. The turbulence values at

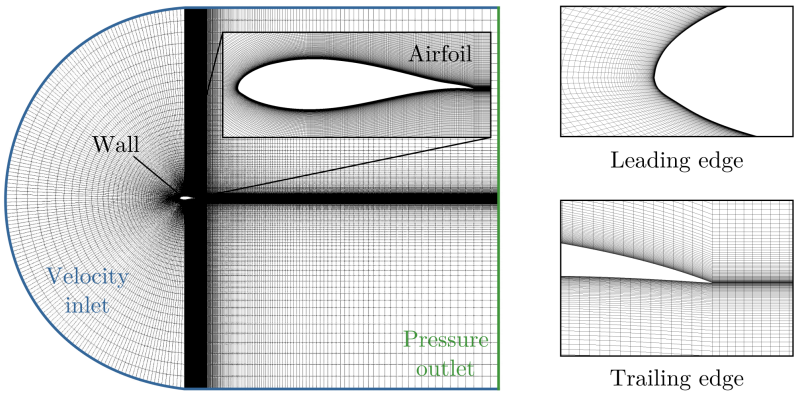

Figure 13: Domain geometry, mesh and boundary conditions of the CFD simulation

the inlet have been calculated as proposed by[15]:

$$k = 0.01 V_\infty^2 \tag{3}$$

$$\omega = 1000 \frac{\rho k}{\mu} \tag{4}$$

obtaining $k = 0.5041\ m^2/s^2$ and $\omega = 3.451 \cdot 10^{-7}\ s^{-1}$.
The coupling algorithm between pressure and velocity is SIMPLE, using the Standard algorithm for the pressure interpolation. Finally, second order upwind schemes have been used to solve the equations of momentum, turbulent kinetic energy and specific dissipation rate. The simulations were performed in a PC with an Intel Celeron J1900 at 1.99 *Ghz* and 4 GB RAM. The convergence criteria were the stabilization of the aerodynamic forces and values of the residuals below 10^{-6}. With these criteria, the mean time for each simulation was around 1.25 *h*.

4.3. Numerical results

4.3.1. Forces on the airfoil

Figure 14 compares the results of the numerical simulations of the proposed airfoil with the results obtained from JavaFoil, confirming that JavaFoil results are trustworthy (although slightly overpredicting both lift and drag) at low angles of attack, below stall angle.

4.3.2. Pressure around the airfoil

Figure 15 shows the normalized pressure contours around the airfoil at the different angles of attack studied.It may be appreciated how, with the increase in the angle of attack, the pressure on the pressure side of the airfoil increases and the pressure on the suction side decreases. For negative angles, the pressure

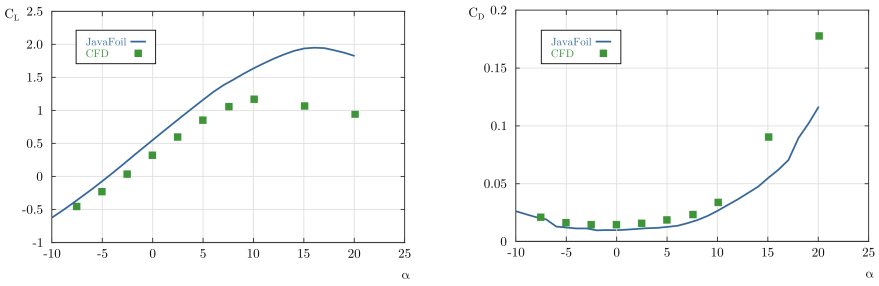

(a) Lift coefficient (b) Drag coefficient

Figure 14: Comparison of JavaFoil and Fluent® results - DU-06-W-200 airfoil

and suction sides interchange. A stagnation point is observed, which moves towards the leading edge with the increase in the angle of attack.

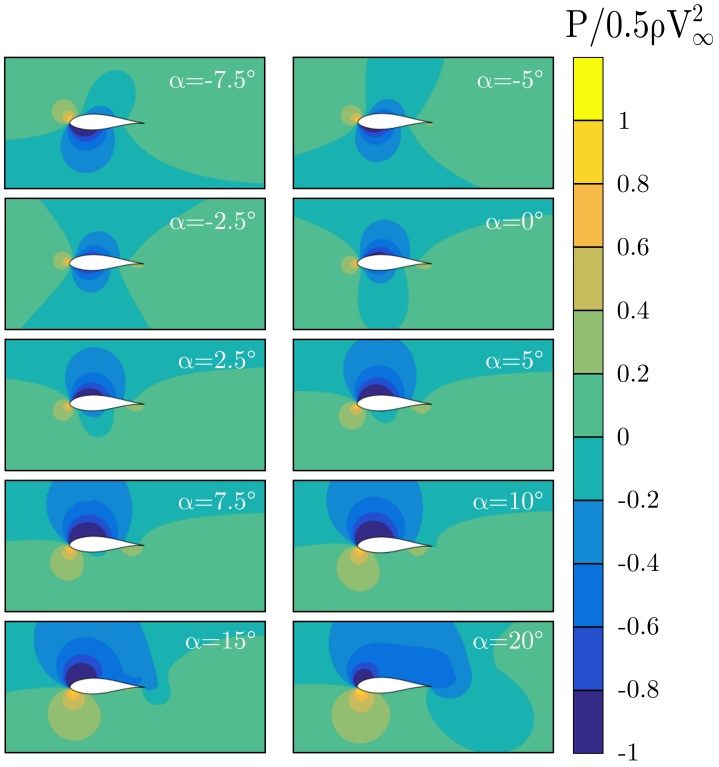

Figure 15: Normalized pressure contours around the UO-17-LDA airfoil at different angles of attack

The pressure coefficients for the different angles of attack studied are shown in Figure 16. It may be observed how the pressure rises near the stagnation point

and how it reaches a minimum in the zones with lower flow velocities.

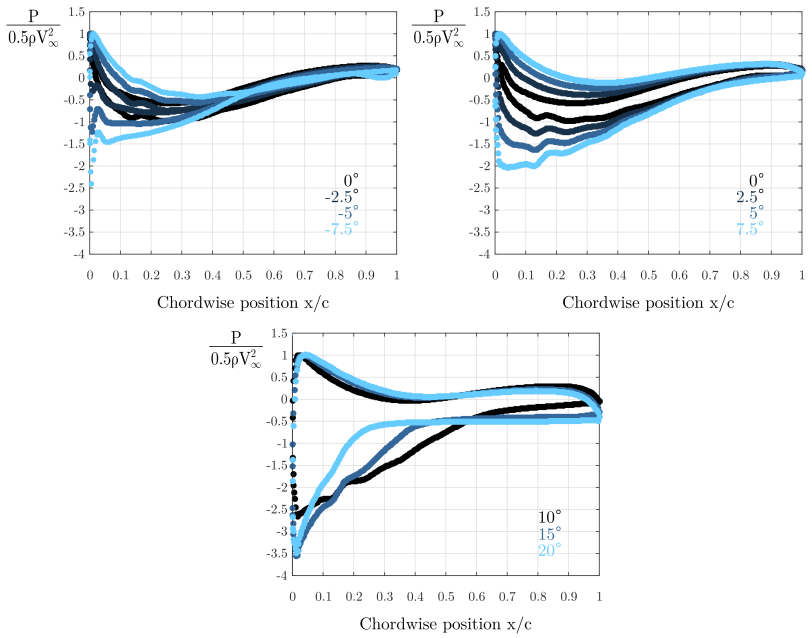

Figure 16: Pressure coefficients of the UO-17-LDA airfoil at different angles of attack

4.3.3. Velocity contours

The normalized velocity contours around the airfoil are depicted in Figure 17. Velocities become higher in the zones of lower pressure around the airfoil. The stagnation point may be identified again, moving as the angle of attack changes. With the increase of the angle of attack, a broadening of the airfoil wake may be as well appreciated. At $\alpha = 15°$, a vortex may be observed in the airfoil wake, which becomes completely detached at $\alpha = 20°$. These results are consistent with the stall angle of the airfoil, which is 16° according to JavaFoil. It must be noted that, at such angles of attack, the unsteady nature of the flow required to perform the CFD simulations unsteadily. The time-step chosen was 0.014 s, which was considered enough to capture all the relevant unsteady effects in the flow, according to the requirements found in [16].

4.3.4. Turbulent kinetic energy contours

Figure 18 shows the turbulent kinetic energy (TKE) contours around the airfoil. Turbulent kinetic energy is calculated as:

$$TKE = \frac{1}{2}\left(\overline{u'u'} + \overline{v'v'}\right) \tag{5}$$

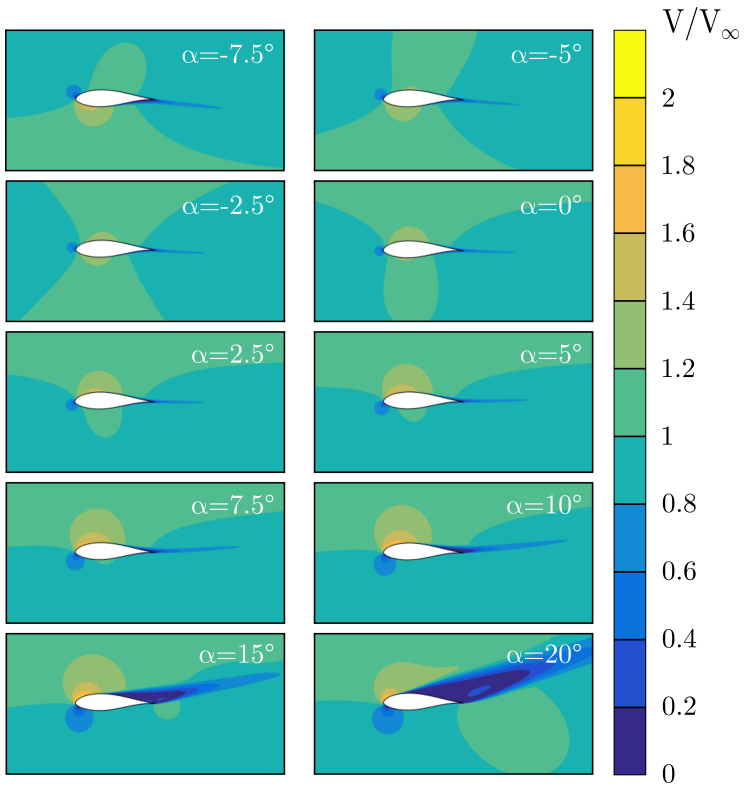

Figure 17: Normalized velocity contours around the UO-17-LDA airfoil at different angles of attack

where u' and v' are the longitudinal and transversal velocity fluctuations. The turbulent kinetic energy in the airfoil wake is a metric of the flow turbulence level. As shown in the velocity contours, the airfoil wake becomes wider with the increase in the angle of attack. At $\alpha = 15°$ and 20°, a dramatic increase of the width of the wake may be observed, confirming the detachment of vortices from the airfoil.

4.3.5. Vorticity contours

Vorticity is a physical magnitude used to quantify the tendency of the flow to rotate. In a 2D simulation, in-plane vorticity is calculated as:

$$\vec{\omega}_z = \left(\frac{\partial v}{\partial x} - \frac{\partial u}{\partial y} \right) \vec{k} \tag{6}$$

where u and v are the velocity components in the longitudinal (x) and transversal (y) directions. At the trailing edge, the wake presents two different colors, with blue representing high negative vorticity values and yellow high positive

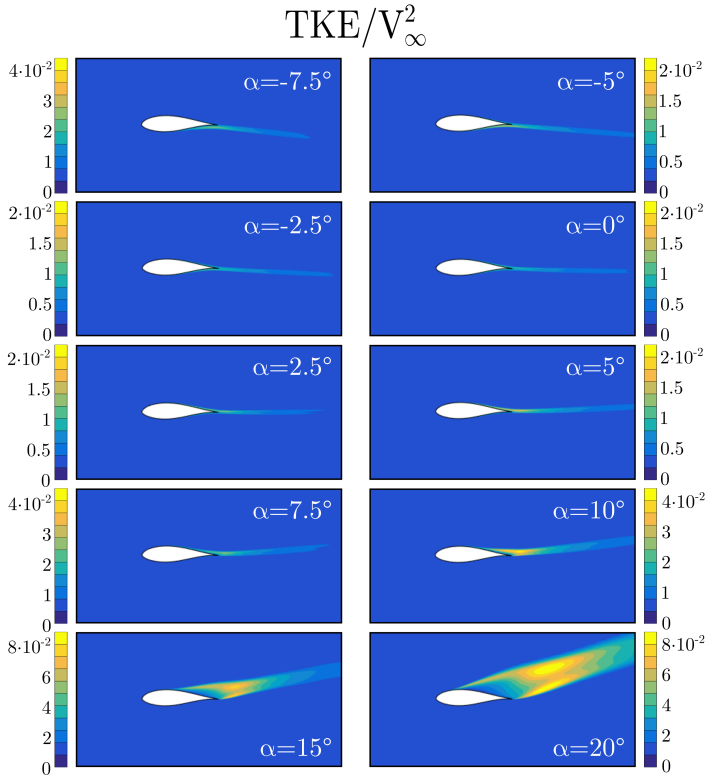

Figure 18: Normalized turbulent kinetic energy contours around the UO-17-LDA airfoil at different angles of attack

ones. Hence, two zones may be identified in the wake, one where the flow tends to rotate in clockwise direction (blue) and one where the flow tends to rotate in counterclockwise direction (yellow). The wake width shows the same behavior as in the velocity and turbulent kinetic energy, increasing with the increase in the angle of attack.

5. Application of the optimized airfoil to VAWT design

Finally, the UO-17-LDA airfoil has been applied to the design of a small-scale VAWT with the following characteristics: After generating the polar lift and drag coefficient data for the original FX-63-137 airfoil and the optimized airfoil UO-17-LDA, the double-multiple streamtube model presented in [17] has been employed to predict the performance of the turbine with the two different airfoils. Figure 20 shows the power coefficient ($C_P = 0.5\rho S V_\infty^2$) of the two designs as a function of the tip speed ratio of the turbine ($\lambda = R\omega/V_\infty$). ρ is the air density, S is the turbine swept area, V_∞ is the incoming wind velocity,

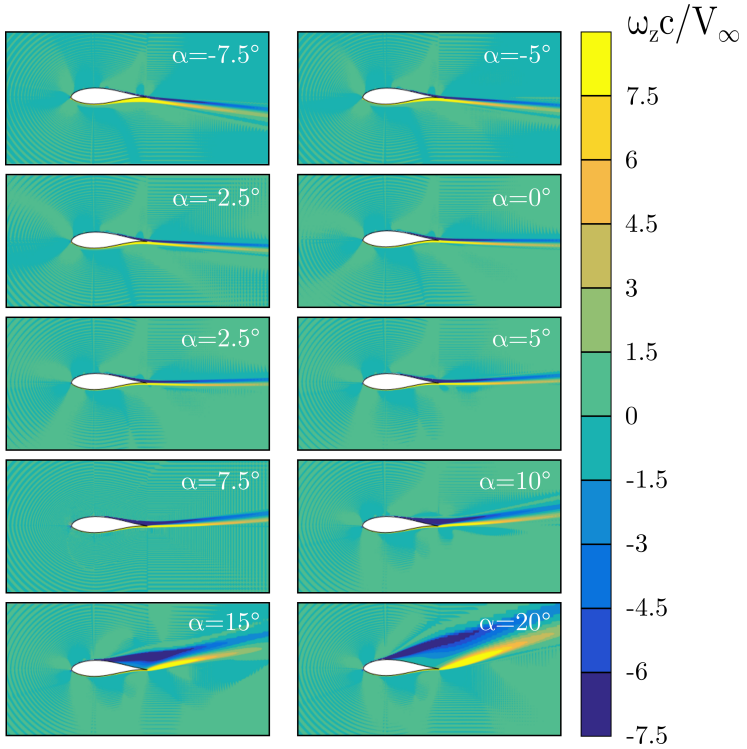

Figure 19: Normalized vorticity contours around the UO-17-LDA airfoil at different angles of attack

Table 3: Characteristics of the analyzed VAWT design

Number of blades N	3
Rotor radius R	1 m
Rotor height H	1 m
Blade chord c	111 mm
Rotor solidity σ	1/3
Nominal wind speed	9 m/s

R is the turbine ratio and ω is the turbine rotational speed. The increase of the performance of the proposed airfoil with respect to the original one may be appreciated. This effect may be ascribed to the delay of stall and the reduction in drag experienced by the UO-17-LDA in comparison with the FX-63-137 airfoil. More specifically, the maximum power obtained with the new airfoil is around 420 W, whereas with the FX-63-137 airfoil this value was around 340 W. Thus, it may be concluded that the proposed airfoil is capable of obtaining better performances in a small-scale VAWT than the original airfoil.
Finally, Figure 21 shows the expected angles of attack during the rotation of the turbine using the proposed airfoil. It may be observed that the angle of attack

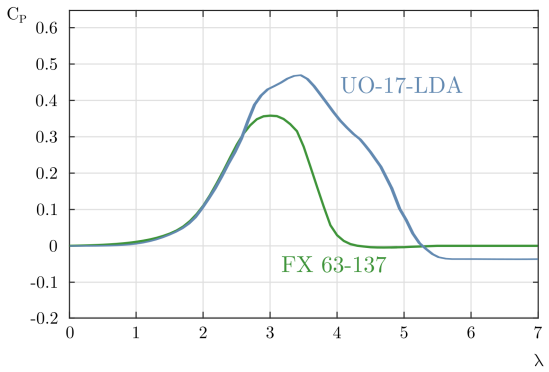

Figure 20: Predicted performance curves of a VAWT using FX-63-137 and UO-17-LDA airfoils and a double-multiple streamtube model

remains well below the stall angle for all the positions at the nominal working point ($\lambda = 3.5$). Thus, all the working points above $\lambda = 3.5$ are correctly modeled by JavaFoil. Besides, until values lower than $\lambda < 2.5$, the percentage of positions with angles of attack outside the range in which JavaFoil predictions are valid is relatively low, so that they are not affecting much to the global power coefficient of the turbine. Therefore, using JavaFoil as the source of airfoil data for the prediction of the $C_P - \lambda$ curve of this VAWT in its useful operational range ($\lambda = 2.5$ to 5) seems a reasonable procedure.

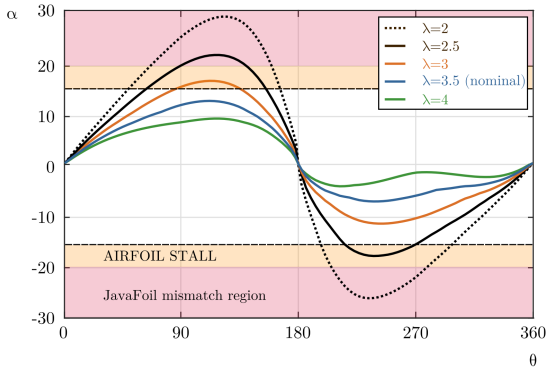

Figure 21: Predicted angles of attack at different blade positions during turbine operation

6. Conclusions

The influence of the geometrical characteristics of an airfoil is determining on its performance. Lift and drag, as well as the stall angle, depend on the thickness and camber of the airfoil, apart from the Reynolds number. In addition,

the positions of maximum thickness and camber also determine the performance of the airfoil. It has been found that thickness values around 18 and 21% and camber values below 4% offer the best results.
The airfoil proposed in this study, UO-17-LDA, is a modification of the FX-63-137 airfoil with the optimum values for thickness and camber found in this work, 21% thickness and 2% camber. A delay in stall of 5° with respect to the original airfoil has been observed using the software JavaFoil, based on a panel method with a coupled boundary layer analysis. The lift coefficient of the proposed airofil is only slightly lower than for the original airfoil, and the increase of the stall angle makes the UO-17-LDA airfoil suitable for its use in vertical-axis wind turbines. The CFD simulations performed for the proposed airfoil are consistent with the predictions of the panel method for lift and drag values. In addition, these simulations have provided insight into the progressive widening of the wake with the angle of attack and the vortex generation that causes the stall of the airfoil. Lastly, the increase of the performance of a VAWT design using the proposed airfoil instead of the original one has been verified using a double-multiple streamtube model.
Finally, comparing the methods employed for the prediction of the airfoil performance, JavaFoil is capable of obtaining results for a wide number of flow conditions in small computational times, with a user-friendly interface. Computational Fluid Dynamic (CFD) simulations with FLUENT® require higher computational times, additionally to the time and effort required to generate the mesh for the simulations. However, the results from JavaFoil are known to diverge from the actual solution at high angles of attack. Hence, JavaFoil is a very useful tool for the prediction of the performance of airfoils at low angles of attack (before stall), as it enables the comparison of different geometries in very small computational times. Nevertheless, the results with CFD are richer and closer to the actual behavior of the airfoil.

Acknowledgment

This work has been supported by the "FPU" predoctoral research scholarship provided by the Spanish Ministry of Education, Culture and Sports. The authors also want to acknowledge the support from the Project "Desarrollo y construcción de turbinas eólicas de eje vertical para entornos urbanos" (ENE2017-89965-P) from the Spanish Ministry of Economy, Industry and Competitiveness.

References

[1] S. Sawyer and K. Rave. Global Wind Report - Annual Market Update. Technical report, Global Wind Energy Council (GWEC), Brussels, Belgium, EU, 2015.

[2] J.F. Manwell, J.G. McGowan, and A.L. Rogers. *Wind Energy Explained: Theory, Design and Application*. John Wiley and Sons, Ltd, Chichester, UK, 2009.

[3] S.J. Kim and J.H. Lee. How biomimetic approach enlarges morphological solution space in a streamlined high-speed train design? In *Proceedings of the 16th Iberoamerican Congress of Digital Graphics (SIGraDI)*, pages 538–542, Fortaleza, Brazil, Nov 2012.

[4] C.T. Foo, B. Omar, and I. Taib. Shape optimization of high-speed rail by biomimetic. In *Proceedings of the International Conference on Mechanical and Manufacturing Engineering (ICME 2017)*, volume 135, Langkawi, Malaysia, Jul 2017. MATEC Web of Conferences.

[5] F.E. Fish and J.M. Battle. Hydrodynamic design of the humpback whale flipper. *Journal of Morphology*, 225:51–60, 1995.

[6] I. Solís-Gallego, D. Menéndez-Alonso, A. Meana-Fernández, J.M. Fernández Oro, K.M. Argüelles Díaz, and S. Velarde-Suárez. Optimization of wind turbine airfoils using geometries based on humpback whale flippers. In *Proceedings of the 6th International Congress of Energy and Environment Engineering and Management (CIIEM15)*, pages 1–4, Paris, France, Jul 2015.

[7] I. Solís-Gallego, A. Meana-Fernández, J.M. Fernández Oro, K.M. Argüelles Díaz, and S. Velarde-Suárez. LES-based numerical prediction of the trailing edge noise in a small wind turbine airfoil at different angles of attack. *Renewable Energy*, 120:241–254, 2018.

[8] J.L. Hess. Panel methods in Computational Fluid Dynamics. *Annual Review of Fluid Mechanics*, 22:255–74, 1990.

[9] Javafoil - analysis of airfoils. `https://www.mh-aerotools.de/airfoils/javafoil.htm`. Accessed: 2018-04-04.

[10] M.C. Claessens. The Design and Testing of Airfoils for Application in Small Vertical Axis Wind Turbines. Master's thesis, November 2006.

[11] E. Castiñeira-Martínez, I. Solís-Gallego, J. González, J.M. Fernández Oro, K.M. Argüelles Díaz, and S. Velarde-Suárez. Application of computational fluid dynamics models to aerodynamic design and optimization of wind turbine airfoils. In *Renewable Energy and Power Quality Journal*, volume 1, pages 370–375, Cordoba, Spain, Apr 2014.

[12] P.G. Tucker. *Unsteady Computational Fluid Dynamics in Aeronautics*. Springer, 2014.

[13] F.R. Menter. Two-equation eddy-viscosity turbulence models for engineering applications. *AIAA Journal*, 32:1598–1605, 1994.

[14] C.D. Argyropoulos and N.C. Markatos. Recent advances on the numerical modelling of turbulent flows. *Applied Mathematical Modelling*, 39:693–732, 2015.

[15] N.N. Sørensen and J.A. Michelsen. Drag prediction for blades at high angle of attack using CFD. *Journal of Solar Energy Engineering*, 126:1011–1016, 2004.

[16] F.M. White. *Fluid Mechanics, 7th Ed.* McGraw-Hill, 2011.

[17] A. Meana-Fernández, I. Solís-Gallego, J.M. Fernández Oro, K.M. Argüelles Díaz, and S. Velarde-Suárez. Parametrical evaluation of the aerodynamic performance of vertical axis wind turbines for the proposal of optimized designs. *Energy*, 147:504–517, 2018.